Paper No.
09292

NACE INTERNATIONAL CORROSION 2009 CONFERENCE & EXPO

CO_2 top of the line corrosion in presence of acetic acid A parametric study

Singer, M.; Hinkson*, D.; Zhang, Z.; Wang***, H.; Nesic, S.**
Ohio University - Institute for Corrosion and Multiphase Technology
342 West State St., Athens, OH 45701

ABSTRACT

This research presents the results of an experimental study of five parameters identified as having a significant influence on Top of the Line Corrosion: partial pressure of CO_2, condensation rate, gas temperature, organic acid concentration and gas velocity. A comprehensive analysis of the effect of each of these five parameters on the type of corrosion is performed. In addition, considerations regarding the importance of the condensation process are discussed.

Keywords: Top of the line corrosion, Condensation, Acetic acid, CO_2 corrosion

INTRODUCTION

The transportation of fluids in pipelines is a critical step in oil and gas production. When it comes directly from the well, the fluid is usually unprocessed and multiphase and can be a mixture of oil, solids, gas and water. The presence of water leads to considerable corrosion problems on the internal walls of the pipelines. The phenomenon of interest in this study is the transportation of wet gas and, more precisely, the Top of the Line Corrosion (TLC) that occurs when significant heat exchange is present between the pipelines and the surroundings (frozen land, deep-sea water). The unprocessed vapor flowing through the pipe condenses on the cold walls, forming a thin film and/or droplets of liquid. The liquid can contain corrosive species such as organic acids and dissolved corrosive gases (such as carbon dioxide or hydrogen sulfide). Therefore the condensation of wet gas can lead to a very corrosive environment.

The first case of TLC observed in the field was reported in the sixties in a sour gas field in France[1]. Since then, numerous cases have been reported, mostly offshore[2,3,4,5] but also on several occasions onshore[6,7]. As it is reported, TLC occurs exclusively in stratified flow regime, at low gas velocity, and in sweet or sour environments. The condensation rate and the presence of organic acid seem to be controlling parameters.

*: Currently at Occidental of Elk Hills, 28590 Highway 119, Tupman, CA 93276
**: Currently at BP America Inc., 501 Westlake Park Blvd., Houston TX 77079
***: Currently at Clariant Corporation, New Trails Drive, The Woodlands TX 77381

In the past twenty years, TLC has been the subject of intensive research. Olsen and Dugstad[8] conducted a systematic experimental study on parameters influencing TLC in sweet conditions. They found that the competition between $FeCO_3$ film formation kinetics and the condensation rates controlled the extent of the corrosion attack. At high temperature (70ºC) and low condensation rate, a dense and protective $FeCO_3$ is favored to form rapidly. At high condensation rate, the saturation in $FeCO_3$ is more difficult to obtain due to the rate of fresh water renewal. DeWaard[9] proposed the first modeling approach to TLC based on his famous full pipe flow empirical equation.

In 1999 Gunaltun[4] added more insight into TLC mechanisms by defining three main zones in the pipeline:
- The bottom of the pipe where the corrosion is uniform and where the rate can be lowered with the use of inhibitors.
- At the sidewall of the pipe where the condensed water drains to the bottom. The corrosion is also uniform but inhibitors are not efficient.
- At the top of the line where a protective iron carbonate layer can be formed in certain cases. Inhibitors are not effective and localized corrosion occurs.

The condensation rate was once again identified as a controlling parameter in TLC and the concept of critical condensation rate grew stronger. It was set at 0.25 $mL/m^2/s$ if the condensation is considered to happen on half of the pipe only. If large quantities of organic acid are present (above 2500 ppm of acetate species), this critical threshold is reduced to 0.025 $mL/m^2/s$ [10].

In 2000, a new model was proposed by Pots[11] which aimed at taking into account the competition between the scale formation rate linked to the iron dissolution and the condensation rate. The so called “Super saturation model” is based on the calculation of the concentration of iron at saturation under film-forming conditions. Pots[11] insisted on the importance of correctly evaluating the condensation rate in order to accurately predict the corrosion rate.

In 2002, Vitse[12,13,14] completed a thorough experimental and theoretical study on the TLC caused by carbon dioxide. Condensation and corrosion experiments were conducted in large scale 4” ID flow loop. Vitse developed two models and adapted them to a top of the line scenario: a mechanistic film-wise condensation model based on Nusselt theory and a semi-empirical corrosion model. The condensation model has a sound mechanistic approach and is based on the assumption that a continuous film of liquid covers the steel surface at the top of the line (film-wise condensation). Vitse acknowledges that while this approach is valid to estimate the condensation rate on the side of the pipe, it is not ideal to cover the condensation process happening at the top (11 to 1 O’clock position) which is drop-wise[4]. Nevertheless, Vitse’s corrosion model constituted a considerable breakthrough in the understanding of the mechanisms involved in TLC.

Between 2002 and 2007, several experimental studies[15,16] were published on the effect of different parameters such as acetic acid, MEG or pH control.

Strong advances in TLC understanding were published in 2007. A series of papers presented additional experimental work and guidelines for field operation[17,18,19]. The same year, Zhang[20] published the first fully mechanistic approach on TLC modeling, covering the three main processes involved in Top of the Line Corrosion phenomena: dropwise condensation, chemistry in the condensed water and corrosion at the steel surface. Most of the experimental data presented in this paper compare well to Zhang’s model[20], which is currently being tested over field data. Zhang’s approach represents one of the most advanced attempts to model the mechanisms involved in TLC to date. It takes into account the most important parameters in CO_2 TLC: condensation rate, gas temperature, CO_2 partial pressure, gas velocity and acetic acid concentration.

Since then, studies have been published on H_2S TLC[21] (experimental work) on the characteristics of the water condensation at the top of the line[22] and on the possible role of hydrocarbon condensate[3].

Remita[23] built upon the work proposed by Vitse[12] and developed a model for CO_2 corrosion under thin liquid film.

Even though much progress has been made over the years on the understanding of TLC mechanisms, none of the models proposed thus far tackle the occurrence and prediction of localized corrosion. The first experimental study focusing on this aspect linked to the TLC phenomena was published by Amri[24], in an effort to relate pit growth and environmental conditions. However, no model has yet been proposed on this topic.

This paper presents some of the TLC experimental work that has been conducted at the Ohio University between the years 2004 and 2007.

EXPERIMENTAL PROCEDURE

The best approach towards understanding any mechanism is to select a baseline condition and to vary one parameter at a time. That is what has been done throughout the work presented here. In addition, some tests have focused on the study of interacting effects between parameters. This approach gives a better insight into the relative weight of each parameter and helps in identifying specific areas of interest where the current understanding remains limited.

The most important five parameters were identified as follows:

- Gas velocity
- Undissociated acetic acid concentration
- Condensation rate
- CO_2 partial pressure
- Gas temperature

One interacting effect is investigated:

- Condensation rate / Acetic acid

Table 1 presents the experimental conditions of the baseline test. Each series of tests proposes a variation of a single parameter around the baseline conditions. Table 2 shows the range of values in which each parameter is varied. Some liquid accumulated at the bottom of the line due to the water condensation forming a small liquid stream. The flow regime could be observed through a high pressure transparent window and was always clearly stratified.
Another important aspect is the wall temperature at the top of the line where the corrosion reaction takes place. This wall temperature is dependant on the gas temperature, the condensation rate and, to lesser extent, the total pressure and the gas velocity. The corresponding values encountered in this experimental study are shown in Table 3. These values are calculated using an approach developed by Zhang[20] which shows very good agreement with experimental measurements.

Large Scale Loop

The experiments were carried out in two similar high temperature, high pressure, 4” ID flow loop. The liquid tank, gas blower, and pipes represent a 30 meter-long system made of stainless steel. Specially-designed test sections enabled the insertion of cylindrical weight loss coupons made of carbon steel. The condensation conditions were simulated using cooling coils wrapped around the pipe. The test section is shown in Figure 1.The condensation rate was measured by collecting the condensed water downstream of the test section. The main liquid phase in the tank is heated to the required temperature using immersion heaters. The vapor phase containing water and acetic acid vapor, CO_2, N_2 is circulated through the pipe to ensure that no liquid from the tank is carried over. A more detailed description of one of the flow loops and its equipment was presented by Singer[15] in 2004.

Liquid Phase Composition

The liquid phase is made up exclusively of de-ionized water; no salt is added. However, dissolved ferrous iron Fe^{2+} build-up occurs throughout the test due to the corrosion process on the weight loss coupons. pH was regularly monitored in the main liquid storage tank and liquid samples were also taken. Although the pH in the main tank did vary between tests from 3.5 to 4.8 depending on the conditions, there is no direct influence on the liquid composition at the top of the line which was always pure condensed water. In fact, the pH in the main tank had to be considered only when evaluating the concentration of free acetic acid.

Scale Formation

There is no easy way to measure the evolution of the pH in the condensed water at the top of the line. The fresh condensed liquid has a relatively low pH, as it is pure water saturated with CO_2. Calculations have shown that the pH can be initially as low as 3 to 3.5. However, as the corrosion process starts, the iron concentration in the condensed droplet rises quickly. Depending on the condensation rate and on the droplet size, conditions for $FeCO_3$ saturation can also be met rapidly inside the droplet.

Acetic Acid Concentration

The acetic acid (HAc) concentration is adjusted by adding a calculated amount of de-oxygenated pure HAc in the tank. The acid will then dissociate to form acetate (Ac^-) and hydrogen ions (H^+). The remaining amount of free acetic acid (which depends on the pH) will define the concentration of total acetic acid present in the condensed liquid at the top of the line. A comprehensive study on the thermodynamics of water/HAc/liquid vapor equilibrium was published by Hinkson[22] in 2007.

Materials Characterization

All of the weight loss coupons are made of API X-65 carbon steel prepared from the same piece of field pipe line (33 cm outside diameter pipe section, 3.8 inch thickness). The chemical analysis of this X65 steel and its microstructure has previously been reported by Singer[25].

Corrosion Rate Measurement

The weight loss coupons were not inserted into the corrosion environment until the system reached steady state. The corrosion rates are measured with weight loss coupons made of API X65 carbon steel. Samples consisting of cylindrical coupons (0.76 cm internal diameter, 3.17 cm external diameter, and 0.5 cm thickness) with an exposed area of 7.44 cm^2 are polished using isopropanol as coolant on silicon carbide papers up to 600 grit. After this preparation, they are covered with liquid Teflon on the outer edges and bottom (Figure 2). Following four to six hours of curing at ambient conditions, the samples are held at 200°C in an oven for four hours. The uncovered steel surface is then re-polished with 600 grit silicon carbide paper wetted with isopropanol, cleaned, dried, and weighed. The coupons are then flush mounted on the internal pipe wall of the loop by using a specially designed probe holder (Figure 2). Therefore, only one face of the coupon is in direct contact with the corrosive environment. The exposure time is between 2 and 21 days in all experiments. Upon removal from the loop, the coupon surface is flushed with isopropanol to dehydrate it and then photographs of the surface are taken. The weight of the coupon after each test is registered, and the ASTM G1 standard procedure is followed to remove the corrosion products and determine the corrosion rate by weight loss. Some coupons are preserved for corrosion product evaluation by scanning electron microscopy (SEM) and energy dispersion analysis (EDS).

Localized Corrosion Characterization

Information on the occurrence and extent of localized corrosion is collected for each test performed using a 3D surface profilometer. It is therefore important to define clearly the parameters measured as follows.

Pitting corrosion: Generally, pits are deep and narrow, and either hemispherical or cup-shaped. When pitting corrosion happens, a part of the material surface undergoes rapid attack while most of the adjacent surface remains unaffected. As described in Figure 3, the criteria used to define pitting corrosion are displayed below:

- the pit depth is 5 times bigger than the general corrosion depth ($b \geq 5a$) ,
- the diameter of pit after film removal is smaller than the pit depth ($c \leq b$).

Mesa attack: Mesa attack is characterized by a wide and often flat-bottomed local attack without protective corrosion film, surrounded by areas with intact corrosion films. Generally, mesa attack starts as several small pits growing beneath the porous corrosion film. These pits can then continue to grow beneath the corrosion film until the lid of corrosion film is torn away by the mechanical forces of flow. Growth of the pits continues by corrosion both laterally and in depth, then the original corrosion film is removed stepwise by the flow. Several such pits can be initiated during a short period of time and grow together into a wide flat-bottomed mesa attack. A galvanic effect between the film-free corroding metal in the bottom of the mesa attack and the film-covered steel outside the mesa attack can increase the corrosion rate in the mesa attack area. As described in Figure 4, the criteria used for mesa attack are:

- the mesa attack depth is 5 times bigger than general corrosion depth ($b \geq 5a$),
- the diameter of mesa is bigger than pit depth ($c \geq b$).

Percentage of coupon surface affected by localized corrosion: Since weight loss steel coupons are used in this study, it was found that the percentage of the coupon surface affected by localized corrosion (pitting and mesa attack together) constitutes an indication of the likelihood of its occurrence.

Experimental Design Flaws and Disclaimer

No laboratory set up can perfectly represent the conditions in the field. While pure corrosion issues have been successfully simulated in small scale set-ups, the flow conditions relative to a 30” ID pipeline are not easily reproducible. Top of the line corrosion is actually as much a corrosion issue as it is a flow regime and heat transfer issue. TLC occurs only in stratified flow, but the way that the condensation process occurs at the top of the line (forming a thin flowing liquid film, or a bigger stagnant droplet) is of prime importance. As it was done in this study, using flat weight loss coupons flush mounted to a cylindrical 4” ID pipe creates conditions leading to preferential condensation and areas where the condensed liquid is trapped artificially (especially at higher gas velocity). On the other hand, using long carbon steel spool pieces is a better representation of the field conditions but it is inconvenient and more costly. In addition, the condensation process happening at the top of a 20” ID pipeline cannot be reproduced perfectly by a 4” ID spool piece because the wall curvature is quite different, leading to unrealistic wetting properties (filmwise instead of dropwise condensation, shorter droplet residence time). This would lead to unrepresentative corrosion scenario. In conclusion, the approach presented in this paper, while being better and more realistic than most previous attempts has the inconvenience of creating “edge” effects in certain conditions. Notwithstanding, the authors believe that the key effects of each influential parameter were successfully determined, but advise that the numerical values of corrosion rate should be used with caution as they are probably conservative estimates.

RESULTS

This chapter presents the corrosion rate results obtained for each of the tests performed. Two types of information are displayed: the evolution of the average (uniform) corrosion rate with time and occurrence of localized corrosion. The average (uniform) corrosion rate is calculated using the weight loss of a coupon and the time of exposure. It gives an average corrosion rate over the entire period of exposure. The localized corrosion graphs present corrosion rates due to pitting or mesa attack and indicate the percentage of surface area of the coupon affected by localized corrosion (pitting or mesa). The corresponding values are obtained by performing a surface analysis on each coupon with a 3D surface profilometer.

The corrosion rate results are displayed in a series of graphs from Figure 6 to Figure 25. Error bars represent the minimum and the maximum values obtained, and the number of coupons (i.e., the number of repeated measurements) is displayed when applicable on each graph.

In CO_2 top of the line corrosion, the uniform corrosion rate usually starts at a high value (several millimeters per year) but in almost every case decreases with time, even over a period of a few weeks. This is due to the formation of $FeCO_3$ on the metal surface. However, the relative protectiveness of this layer will be affected by the experimental conditions, especially concentration of acetic acid or condensation rate.

Influence of the CO_2 Partial Pressure

In general, the higher the partial pressure of CO_2, the higher the uniform corrosion will be, as shown in Figure 6. A protective $FeCO_3$ film forms on the surface of the coupon and leads to a decline of the corrosion attack after 18 days of testing at 2 bars partial pressure of CO_2 and above. At lower partial pressure of CO_2 (0.13 bar), the conditions of $FeCO_3$ supersaturation seem to be more difficult to reach, and the protective film does not form correctly, leading to a low but constant corrosion rate over time (around 0.4 mm/year). At higher partial pressure of CO_2, the corrosion attack is initially more aggressive but the uniform corrosion rate decreases with time to reach 0.3 mm/year after 21 days of testing. Since all the conditions of $FeCO_3$ supersaturation are met easily (high Fe^{2+} and CO_3^{2-} concentration), a dense protective film forms on the metal surface. Pitting corrosion was observed at partial pressures of 2 and 7 bars and stronger at 7 bars partial pressure of CO_2 (Figure 7). Weaker pitting was observed at 0.13 bars partial pressure of CO_2 after 21 days of testing. In the case of CO_2 top of the line corrosion, the occurrence of localized corrosion is strongly linked with the presence of a protective $FeCO_3$ layer which undergoes some breakdown due to higher local corrosivity. The change of corrosivity in the condensed liquid is due to the condensation process itself, which sees droplets of liquid nucleate grow and eventually fall because of gravity forces. During this process, the chemistry in the droplet undergoes a significant increase in pH and in Fe^{2+} concentration which favors scale formation. Once the droplet reaches its maximum size and falls, a new droplet will form with lower pH and more aggressive corrosivity. The cycle is believed to challenge the protectiveness of the $FeCO_3$ layer and lead to localized corrosion.

Influence of Gas Velocity

The most visible influence of gas velocity appears on the condensation regime which, in return, will affect the way the corrosion process occurs. At low velocity (<5 m/s), the vapor condenses by forming stagnant droplets at the top of the pipe (see

Figure **5**). In these stagnant droplets, the $FeCO_3$ supersaturation can be very high, enabling the formation of a dense protective layer. As the gas velocity increases, the condensation regime switches gradually from stagnant to sliding droplet. In the sliding droplet mode, the droplets of condensed liquid flow along the top of the pipe and eventually slide to the bottom. The sliding droplets are not generally in contact with the pipe steel long enough to create a $FeCO_3$ film (as

opposed to the stagnant droplet condensation regime). Instead, a thick but non-protective Fe_3C forms on the liquid pathways that the sliding droplets create. It leads to the formation of two different types of film at the top of the line: protective $FeCO_3$ on most of the coupon area and non-protective Fe_3C on the preferential liquid pathways. Figure 9 clearly shows these preferential liquid pathways for a gas velocity of 10 m/s. The weight loss method does not differentiate between the types of film and gives an average corrosion rate over the entire surface of the coupons. It is possible to correct the space average corrosion rate by evaluating the percentage of surface coverage of both types of film on the coupon surface. However, this process can lead to a high margin of error and does not bring any valuable additional information. Under the Fe_3C layer, the average corrosion rate can be as high as 10 mm/year (similar to what would happen at the bottom of the line). Under the parts of the coupons covered by a $FeCO_3$ layer, the situation resembles a typical TLC scenario with a much lower uniform corrosion rate. Some localized corrosion was observed in every test on the parts covered by $FeCO_3$. The corrosion under Fe_3C film is usually uniform. There was no clear influence of the gas velocity on the extent of the localized corrosion. The space average corrosion rate results do not appear in this paper as they do not help in clarifying this particular phenomenon. There was no visible effect of the gas velocity on the top of the line corrosion (uniform and localized corrosion) except for the change in condensation regime discussed earlier.

Rough observations made during the experiment showed that the condensation regime starts to change from stagnant droplet to sliding droplet at a gas velocity around 10 m/s (rivulets of liquid form on the coupon surface) for a total pressure of 3 bars. Since then, a more comprehensive effort to understand and predict the transition zone between stagnant and sliding droplet has been made. A model developed by Zhang[20] was presented in 2006 and constitutes a good predictive tool for this kind of scenario.

In summary, once the condensation regime switches from stagnant to sliding droplet, parts of the coupon at the top of the line start to be heavily corroded at a rate similar to that at the bottom of the line. However, the flow regime is not yet annular (which happens in our experimental conditions around 20 m/s) as the droplets flowing at the top are still exclusively made of pure condensed water saturated with CO_2. Defining this transition zone is therefore crucial. Additional issues related to droplet transport from the bottom to the top of the line may be expected at high gas velocity. However, no inquiry was made into this phenomenon during the study.

Influence of the Concentration of Undissociated Acetic Acid

The presence of 100 ppm of free acetic acid in the liquid phase of the tank does not seem to have a strong impact on the average corrosion rate (Figure 10). The contribution to the overall cathodic reaction of such a small amount is also minimal. However, as the free acetic acid concentration is increased to 1000 ppm, the average corrosion rate doubles at every point in time. The corrosion rate is still at 2 mm/year after 3 weeks of testing. Moreover, even though traces of localized corrosion were found in tests performed, the presence of acetic acid strongly promotes the occurrence of pitting corrosion proportional to the amount of acid in the solution (Figure 11). With 1000 ppm of free acetic acid, the pitting rate is 7.5 mm/year after 3 weeks of testing. Once again, the presence of a protective layer, together with a local change in chemistry and pH (due to the continuous renewal of condensed droplet), are believed to be responsible for the occurrence of localized corrosion. Acetic acid, being a volatile weak acid, increases the corrosivity of the condensed water and challenges the integrity of the $FeCO_3$ layer (Figure 12).

Influence of the Condensation Rate

The average corrosion rate is expected to be lowest at the lowest condensation rate (Figure 13). The reason is that the rate of renewal of condensed droplets is faster at higher condensation rates. The saturation of $FeCO_3$ is easier to achieve when droplets of liquid remain attached to the metal surface for a longer time. Nevertheless, no significant difference in the average uniform corrosion

rate between 0.03 and 1 ml/m^2/s was found in this study. The corrosion rates are very similar over time and, in all cases, the corrosion attack seems to stop after 20 days due to the formation of a protective $FeCO_3$ scale at the surface of the steel. This is unexpected, since a higher condensation rate is usually synonymous with a higher general corrosion rate, at least at the beginning of the test. In all cases, the condensation regime seems to be stagnant droplet condensation. The influence of the condensation is much stronger on the localized attack (Figure 14). Both pitting rate and surface coverage by localized attack increase dramatically with the condensation rate. Figure 15 shows one of the weight loss coupons exposed for 21 days to the baseline environment and a condensation rate of 1 ml/m^2/s. The corrosion product layer has been removed and the steel surface presents numerous localized corrosion features. Mesa attack seems to be predominant in this case with wide pits easily identifiable.

Influence of the Gas Temperature

Since the corrosion reactions respond to temperature according to by Arrhenius type laws, the average corrosion rate decreases as the gas temperature decreases (Figure 16). This is usually true in full pipe flow, where there is no protective film forming at the surface of the steel. It is, however, different at the top of the line, as the presence of a protective layer plays a role as well. In the first days of testing, the corrosion rate is higher (70°C compared with 40°C). However, as time goes by, the corrosion rate at 70°C decreases strongly, while the corrosion rate at 40°C does not. After 15 days, the corrosion rate at 70°C test has reached the same value as 40°C; after 20 days, it has stopped. In contrast, at 40°C the corrosion rate starts at a low value (0.5 mm/year) but remains almost constant throughout the test. This is explained by the properties of the film forming at the surface of the steel: a dense and protective $FeCO_3$ layer at 70°C and a more porous and less-protective $FeCO_3$ layer at 40°C. The same reasoning applies for the test at 85°C, where it starts at the highest value (above 1.5 mm/year) and strongly decreases with time to reach 0.5 mm/year after 17 days. The corrosion product film is expected to be denser and more protective at a higher temperature since the kinetics of $FeCO_3$ precipitation are faster. Moreover, at the top of the line, there was no sign of localized corrosion at 40°C or 85°C while there was strong evidence of pitting at 70°C (Figure 17). It is clear that the properties of the corrosion product film (rate of formation, density, integrity) are strongly linked to the occurrence of localized corrosion.

Combined Effect of the Condensation Rate and the Acetic Acid Concentration

For clarity purposes, the results are presented in four sets of graphs isolating one parameter each time:

- Set 1: Fixed undissociated acetic acid concentration= 100 ppm and varying Condensation rate = 0.03, 0.25 and 1 mL/m^2/s
- Set 2: Fixed undissociated acetic acid concentration= 1000 ppm and varying Condensation rate = 0.03, 0.25 and 1 mL/m^2/s
- Set 3: Fixed Condensation rate = 0.05 mL/m^2/s and varying undissociated acetic acid concentration = 0, 100, 1000 ppm
- Set 4: Fixed Condensation rate = 1 mL/m^2/s and varying undissociated acetic acid concentration = 0, 100, 1000 ppm

The graphs related to each set are presented in Figure 18 to Figure 25. The clearest observation is that the higher the concentration of free acetic acid and thecondensation rate are, the higher the risk for localized corrosion. Even if the condensation rate is low (0.05 ml/m^2/s), 1000 ppm of free HAc will lead to high uniform corrosion rate and severe localized attack (Figure 26). The opposite is also true for the condensation rate but to a slightly lower extent. The notion of critical threshold condensation rate below which no TLC is expected (or where the TLC rate is acceptable) is not validated by these results. The condensation is clearly a factor influencing the uniform corrosion and localized corrosion rate but cannot be extracted alone and used as a design tool. The extent of TLC is rather the result

of complex interactions between all the parameters presented in this paper and any comprehensive mitigation method requires a good understanding of the mechanisms involved.

CONCLUSIONS

Influence of the CO_2 Partial Pressure (Range from 0.13 to 8 bars)

- At the top of the line, the initial corrosion rate increases with the partial pressure of CO_2.

Influence of the Condensation Rate (Range from 0.03 to 1 ml/m^2/s)

- The initial corrosion rate seems to increase slightly with the condensation rate. However, the condensation rate does not seem to have any influence on the final corrosion rate at the top of the line.
- The condensation rate has a major influence on localized corrosion occurrence and extent.

Influence of the Acetic Acid Concentration (Range from 20 to 1000 ppm of un-dissociated HAc)

- The presence of acetic acid increases the initial corrosion rate at the top of the line.
- The acetic acid can strongly affect the final corrosion rate at the top of the line depending on the amount of acid present. The influence of the concentration of free acetic acid is not insignificant at 100 ppm while it is strong at 1000 ppm. Moreover, in a CO_2 environment, it strongly promotes localized corrosion.

Influence of the Gas Velocity (Range from 5 to 15 m/s)

- At a gas velocity of 5 m/s or below, the flow regime is clearly stratified and the condensation regime is stagnant droplet.
- At a gas velocity between 10 and 15 m/s, the condensation regime starts to switch from stagnant droplet to sliding droplet, leading to a high general corrosion rate at the top of the line.
- Above 15m/s the flow regime changes gradually from stratified flow to annular flow.
- The gas velocity does not have a significant impact on localized corrosion.

Influence of the Gas Temperature (Range from 40 to 85°C)

- The initial corrosion rate at the top of the line is lower at a lower temperature (from 40°C to 85°C).
- At a gas temperature of 40°C, the general corrosion rate at the top of the line remains constant at a fairly low value throughout the test.
- As the temperature increases, the corrosion product film ($FeCO_3$) becomes denser and more protective. Localized attack was observed only at 70°C.

Influence of the Test Duration

- The average corrosion rate at the top of the line strongly decreases with time. It is usually very different at the beginning and at the end of the test.
- In researching localized corrosion, any test shorter than 2 weeks is of limited value.

Localized Corrosion Occurrence

- In sweet conditions, localized corrosion was only observed for the tests performed at 70°C, regardless of gas velocity, condensation rate or acetic acid concentration.
- The presence of acetic acid can greatly promote pitting. The effect seems to be proportional to the amount of acid present.
- Similarly, a high condensation rate also promotes greater localized corrosion.

ACKNOWLEDGEMENTS

The authors would like to express their gratitude to Total, BP, ConocoPhillips, Chevron, Saudi Aramco, Occidental Oil Company and ENI for their support of this research and for allowing the publication of this paper. The authors are also grateful to Georges Harris (ConocoPhillips laboratories) for his help regarding surface profile analysis, and Bruce Brown and Alvaro Camacho, current and former colleagues at the Institute, for their contributions to this experimental work.

REFERENCES

1. Paillassa R., Dieumegard M., Estevoyer M., “Corrosion control in the gathering system at Lacq sour gas field”, 2nd Intl. Congress o Metallic Corrosion, NACE, pp 410-417, New York, 1963.
2. Gunaltun Y.M., Supriyataman D., Jumakludin A., “Top of the line corrosion in multiphase gas line. A case history”, Corrosion/99, paper# 36.
3. Thammachart M., Gunaltun Y., Punpruk S., “The use of inspection results for the evaluation of batch treatment efficiency and the remaining life of the pipelines subjected to top of line corrosion”, Corrosion/08, paper# 8471.
4. Gunaltun Y., Larrey D., “Correlation of cases of top of the line corrosion with calculated water condensation rates”, Corrosion/00, paper# 71.
5. Piccardino J.R., Stuvik M., Gunaltun Y., Pornthep T., “Internal inspection of wet gas line subject to top of line corrosion”, Corrosion/04, paper# 4354.
6. Edwards M., Cramer B., “Top of the line corrosion –Diagnostic, root cause analysis and treatment”, Corrosion/00, paper# 72.
7. Ho-Chung-Qui D.F., Williamson A.I., Eng P., “Corrosion experiences and inhibition practices in wet sour gathering systems”, Corrosion/87, paper# 46.
8. Olsen S., Dugstad A., “Corrosion under dewing conditions”, Corrosion/93, paper# 472.
9. DeWaard C., Lotz U., Milliams D.E., “Predictive model for CO_2 corrosion engineering in wet natural wet gas pipelines”, Corrosion, 47(12), p 976-985, 1991.
10. Gunaltun Y., Piccardino R., Vinazza D., “Interpretation of MFL and UT inspection results in case of top of line corrosion”, Corrosion/06, paper# 6170.
11. Pots B.F.M., Hendriksen E.L.J.A., “CO_2 corrosion under scaling conditions – The special case of top-of-the-line corrosion in wet gas pipelines”, Corrosion/00, paper# 31.
12. Vitse F., Gunaltun Y., Larrey de Torreben D., Duchet-Suchaux P., “Mechanistic model for the prediction of top-of-the-line corrosion risk”, Corrosion/03, paper# 3633.
13. Vitse F., Khairul A., Gunaltun Y., Larrey de Torreben D., Duchet-Suchaux P., “Semi-empirical model for prediction of the top-of-the-line corrosion risk”, Corrosion/02, paper# 2245.
14. Vitse F., “Experimental and theoretical study of the phenomena of corrosion by carbon dioxide under dewing conditions at the top of a horizontal pipeline in presence of a non-condensable gas”, Ohio University, PhD Dissertation, 2002.
15. Singer M., Nesic S., Gunaltun Y., “Top of the line corrosion in presence of acetic acid and carbon dioxide”, Corrosion/04, paper# 4377.
16. Mendez C., Singer M., Camacho A., Hernandez S., Nesic S., “Effect of acetic acid, pH and MEG on CO_2 top of the line corrosion”, Corrosion/05, paper# 5278
17. Halvorsen A.M.K.., Andersen T., Halvorsen E., Kojen G., Skar J., “The relationship between internal corrosion control method, scale formation, and MEG handling of a multiphase carbon steel carrying wet gas with CO_2 and acetic acid”, Corrosion/07, paper# 7313.
18. Andersen T., Halvorsen A.M.K., A. Valle A., Kojen G., “The influence of condensation rate and acetic acid concentration on TOL corrosion in multiphase pipelines”, Corrosion/07, paper# 7312.
19. Nyborg R., Dugstad A., “Top of the line corrosion and water condensation artes in wet gas pipelines”, Corrosion/07, paper# 7555.
20. Zhang Z., Hinkson D., Singer M., Wang H., Nesic S., “A mechanistic model for Top of the line corrosion”, Corrosion, 63(11), 1051-1062, 2007 or Corrosion/07, paper# 7556.
21. Camacho A., Singer M., Brown B., Nesic., “Top of the Line Corrosion in H_2S/CO_2 Environments”, Corrosion/08, paper# 8470.

22. Hinkson D., Singer M., Zhang Z., Nesic S., “A study of the chemical composition and corrosivity of the condensate in top of the line corrosion”, Corrosion/08, paper# 8466.
23. Remita E., Tribollet B., Sutter B.,Ropital F., Longaygue X., Kittel J., Taravel-Condat C., Desamaise N.,“A kinetic model for CO_2 corrosion in confined aqueous environments”, Journal of the Electrochemical Society, 155(1), C41-C45, 2008.
24. Amri J., Gulbrandsen E., Nogueira R.P., “The effect of acetic acid on the pit propagation in CO_2 corrosion of carbon steel”, Electrochemistry Communications, 10, 200–203, 2008.
25. Singer M., Brown B., Camacho A., Nesic S., “Combined effect of CO_2, H_2S and acetic acid on bottom of the line corrosion”, Corrosion/07, paper# 7661.

Table 1: Baseline conditions

Parameters	Baseline conditions
Absolute pressure (bar)	*3*
pCO_2 (bar)	*2*
Gas temperature (°C)	*70*
Condensation rate (mL/m^2/s)	*0.25*
Gas velocity (m/s)	*5*
pH_2S (bar)	*0*
Free HAc concentration in the tank (ppm)	*0*
Steel type	API X65
Liquid phase composition	DI water
pH (tank)	4.5
Test duration (weeks)	3

Only the value of the parameters in italic will be varied on this study

Table 2: Range of variables

Parameters	Range		
	Min	Medium	Max
Absolute pressure (bar)	3	3	8
pCO_2 (bar)	0.13	2	8
Gas temperature (°C)	40	70	90
Condensation rate (mL/m^2/s)	0.05	0.25	1
Gas velocity (m/s)	5	10	15
Free HAc concentration in the tank (ppm)	0	100	1000

NB: The absolute pressure is not varied independently of the CO_2 partial pressure

Table 3: Wall temperature

Gas temperature (°C)	Condensation rate (mL/m^2/s)	Total pressure (bar)	Wall temperature (°C)
70	0.03	3	69.8
70	0.25	3	68.2
70	1	3	63.2
40	0.25	3	33.5
70	0.25	0.13	68.3
70	0.25	8.3	67.8

Figure 1 - Typical TLC Test section

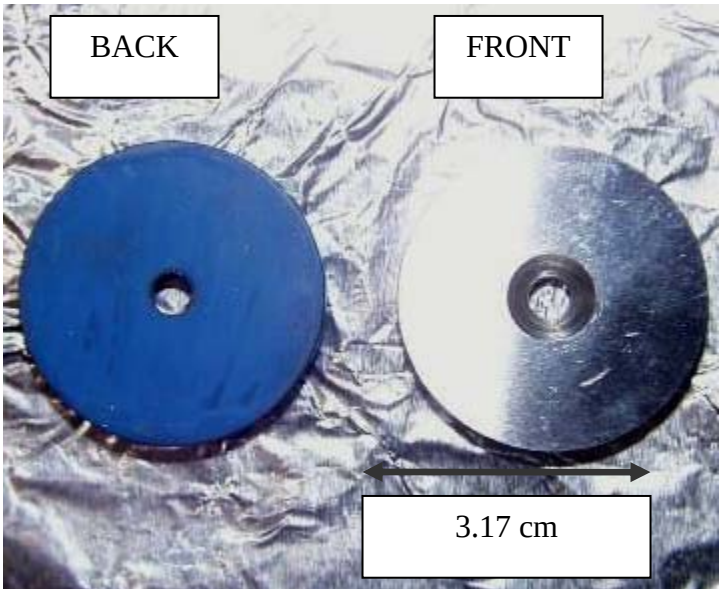

Weight loss coupons with Teflon coating at the back and the side

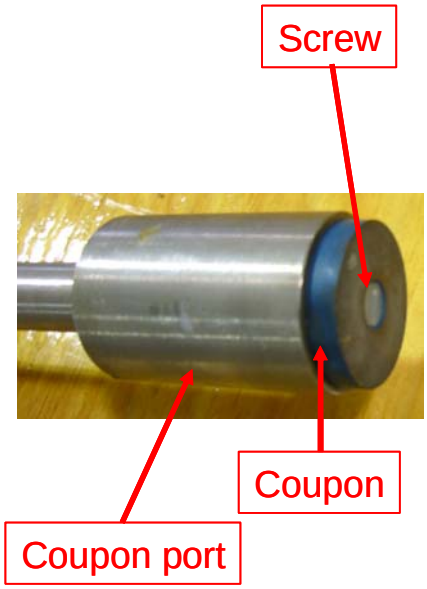

Coupon holder configuration

Figure 2 - Weight loss coupon design

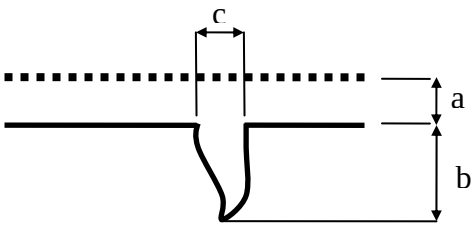

a: general corrosion depth
b: pit depth after film removal
c: diameter of pit after film removal

Figure 3: Schematic representation of pitting corrosion

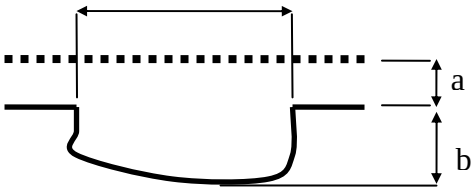

a: general corrosion depth
b: pit depth after film removal
c: diameter of pit after film removal

Figure 4: Schematic representation of mesa attack

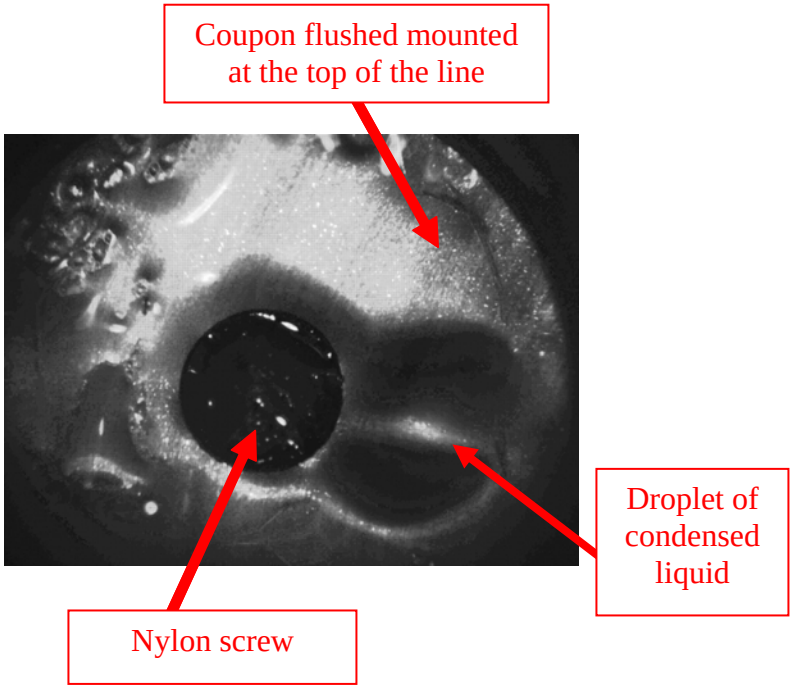

Figure 5: View of the weight loss coupon at the beginning of test taken via a port installed at the bottom of the line

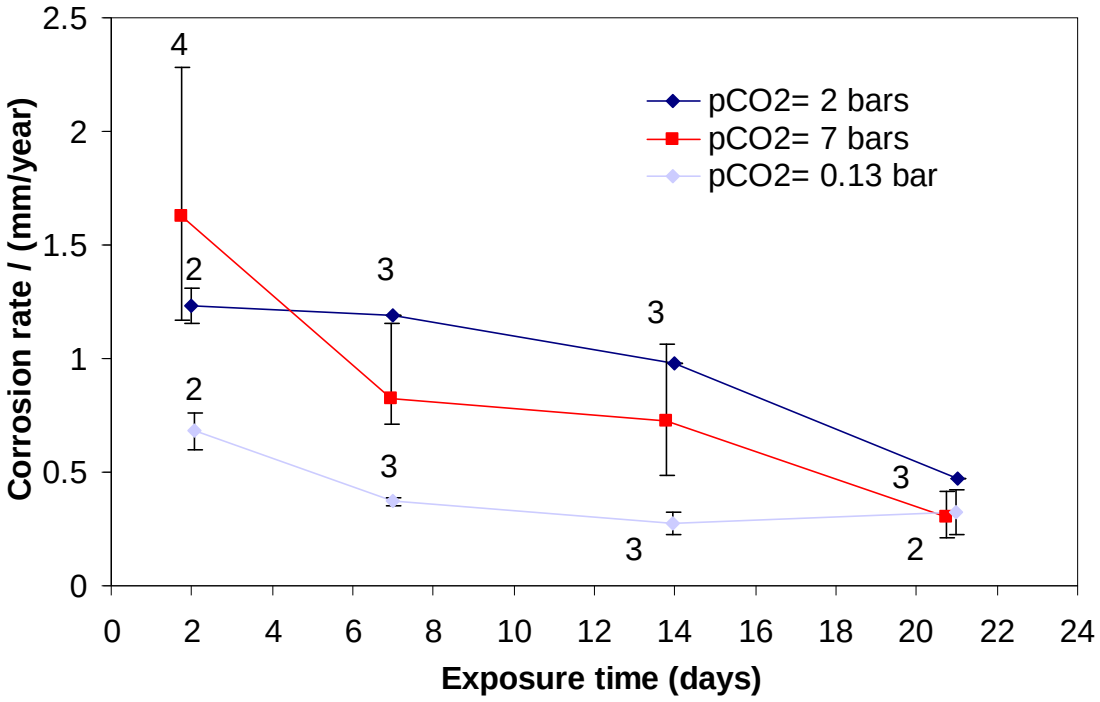

Figure 6: General corrosion – Effect of the pCO_2
T_g=70°C, $[HAc]_{free}$=0ppm, V_g=5m/s, Condensation rate=0.05 mL/m²/s

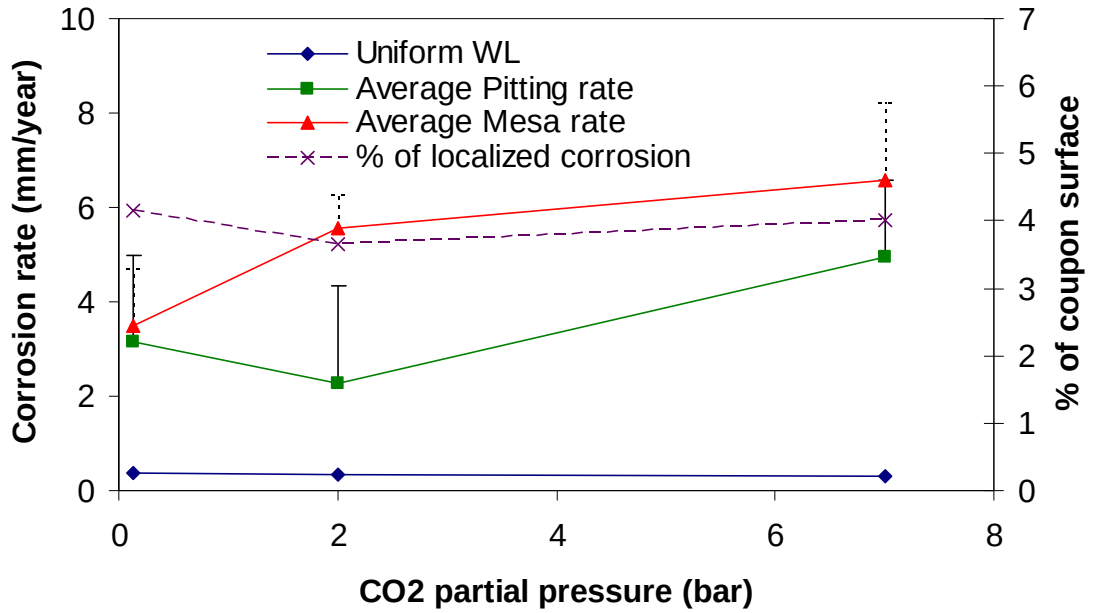

Figure 7: Localized corrosion - Effect of the pCO_2
T_g=70°C, $[HAc]_{free}$=0ppm, V_g=5m/s, Condensation rate=0.05 mL/m²/s

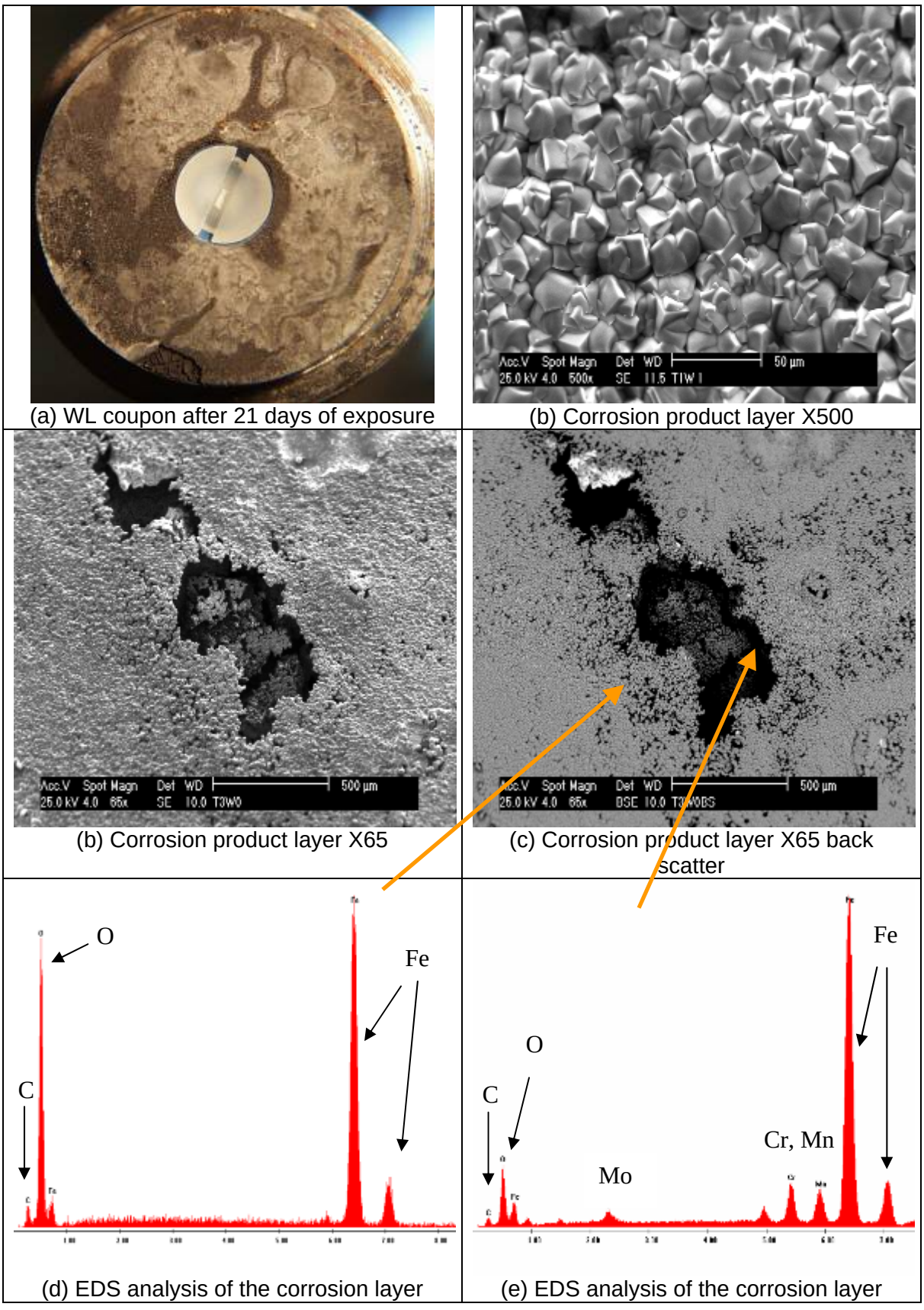

Figure 8 – Surface analysis with corrosion product / pCO_2= 2 bars (P_T: 3 bars, Vg= 5 m/s, Free HAc: 0 ppm, T_g: 70°C, condensation rate= 0.25 mL/m^2/s)

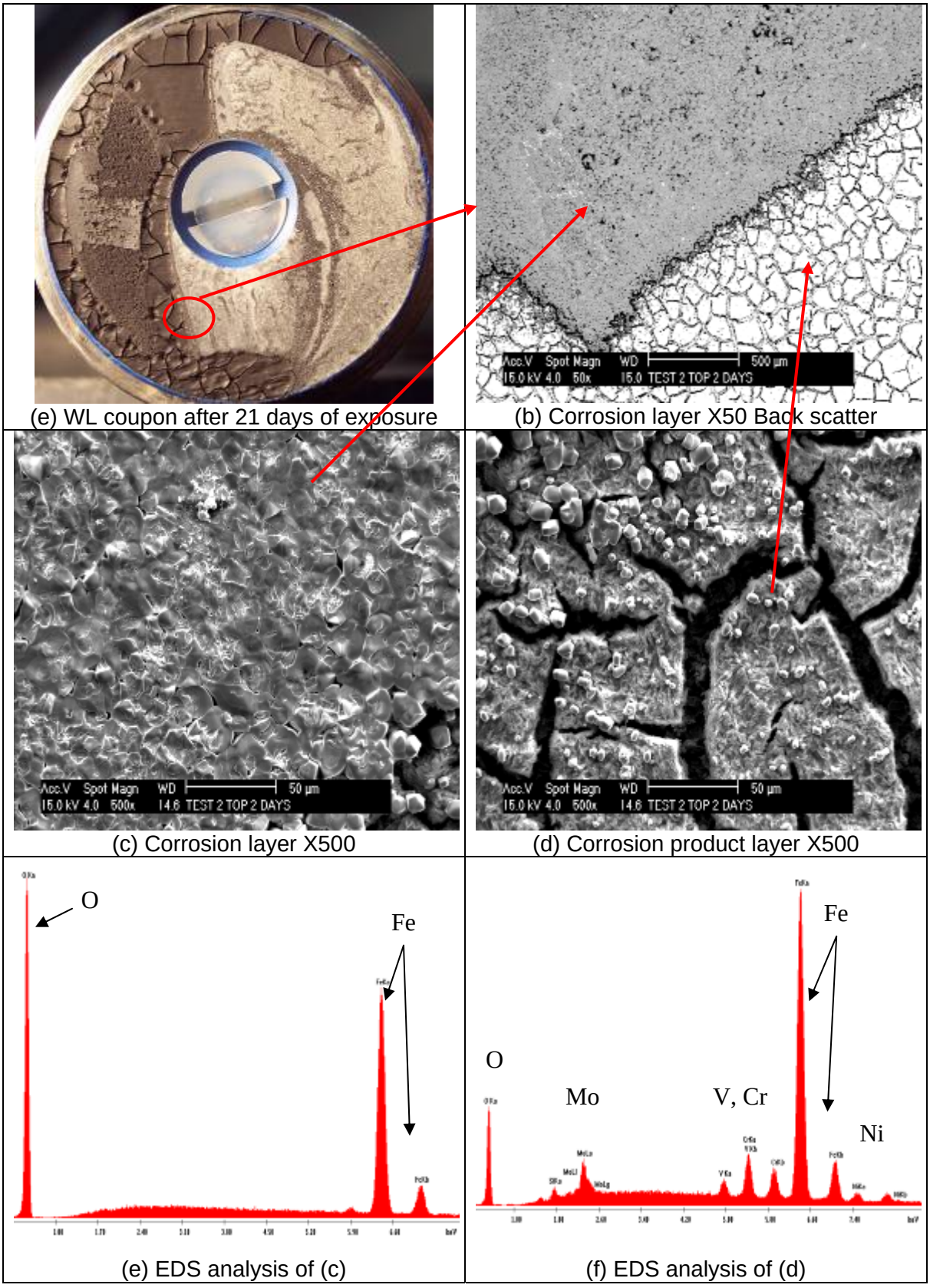

(e) WL coupon after 21 days of exposure

(b) Corrosion layer X50 Back scatter

(c) Corrosion layer X500

(d) Corrosion product layer X500

(e) EDS analysis of (c)

(f) EDS analysis of (d)

Figure 9 – Surface analysis with corrosion product / Vg=10m/s
(P_T: 3 bars, pCO_2: 2 bars, Free HAc: 0 ppm, T_g: 70°C, condensation rate= 0.25 mL/m^2/s)

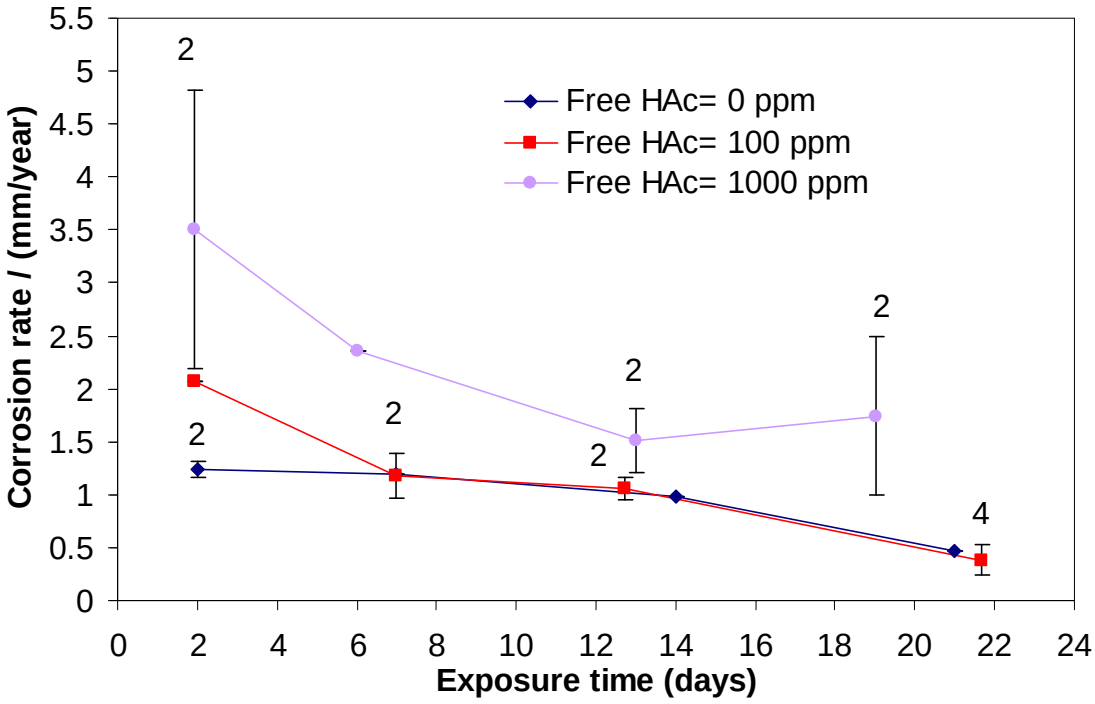

Figure 10: General corrosion - Effect of the free HAc concentration pCO_2=3bars, T_g=70°C, Condensation rate=0.05 mL/m²/s, V_g=5m/s

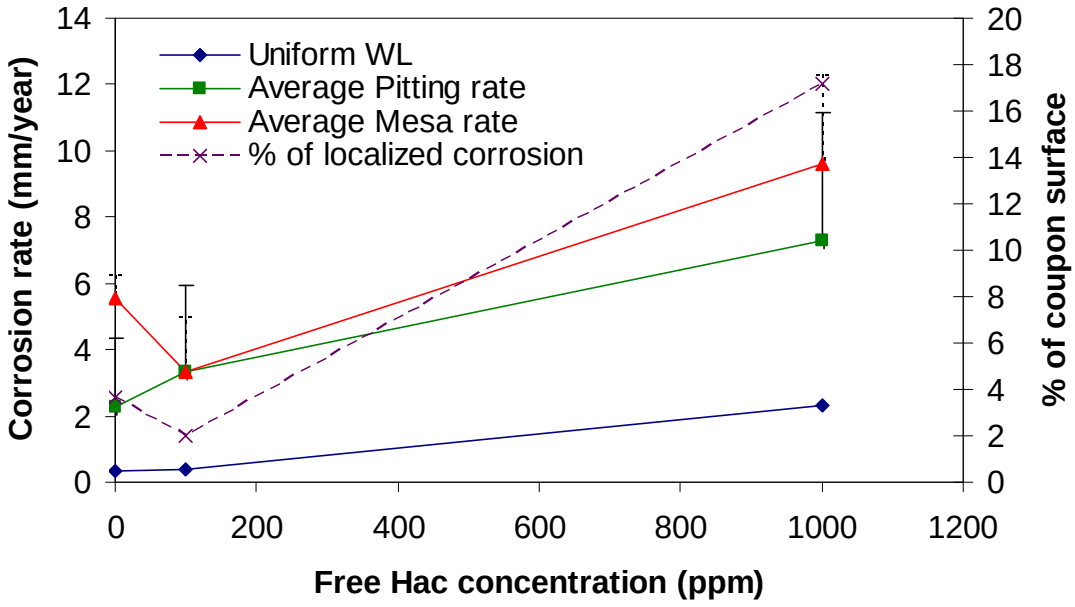

Figure 11: Localized corrosion - Effect of the free HAc concentration pCO_2=3bars, T_g=70°C, Condensation rate=0.05 mL/m²/s, V_g=5m/s

(a) WL coupon after 21 days of exposure

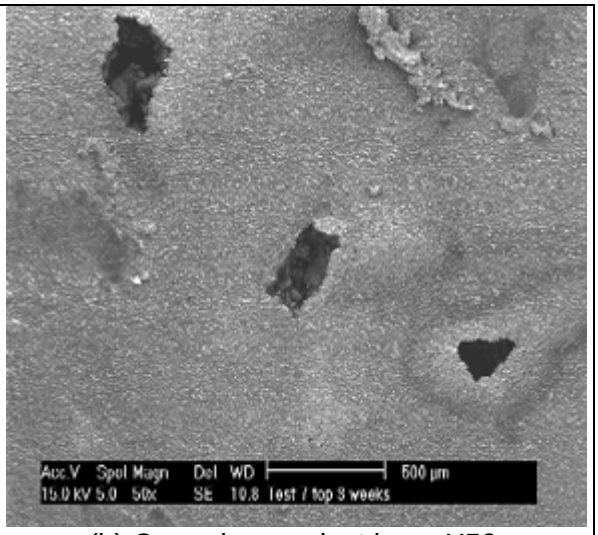

(b) Corrosion product layer X50

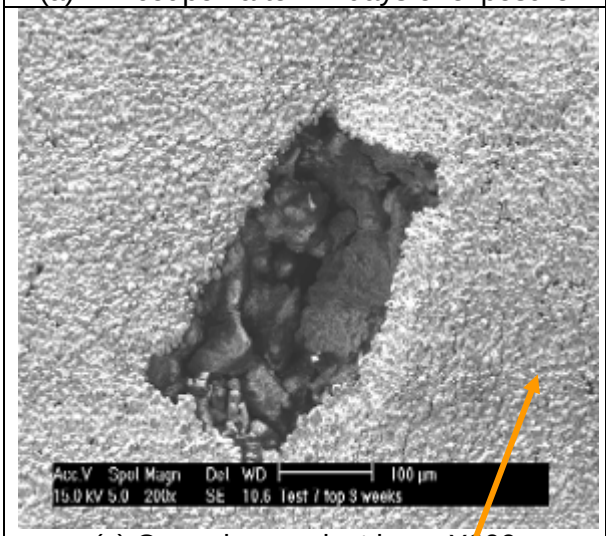

(c) Corrosion product layer X200

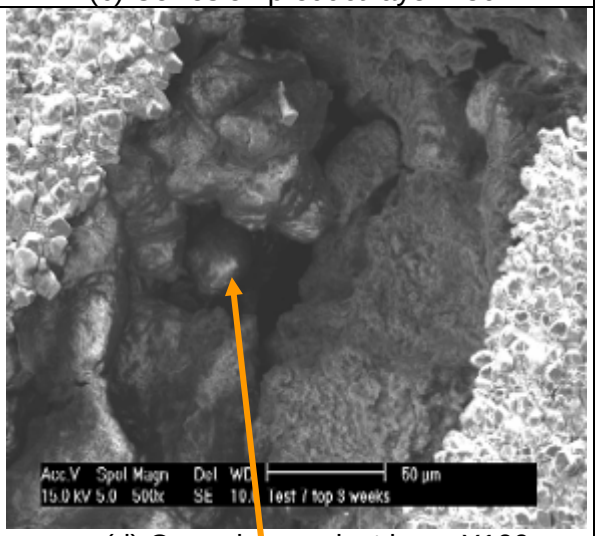

(d) Corrosion product layer X100

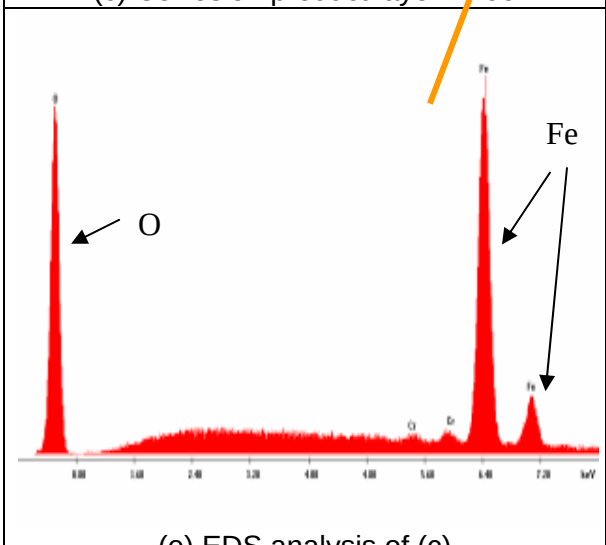

(e) EDS analysis of (c)

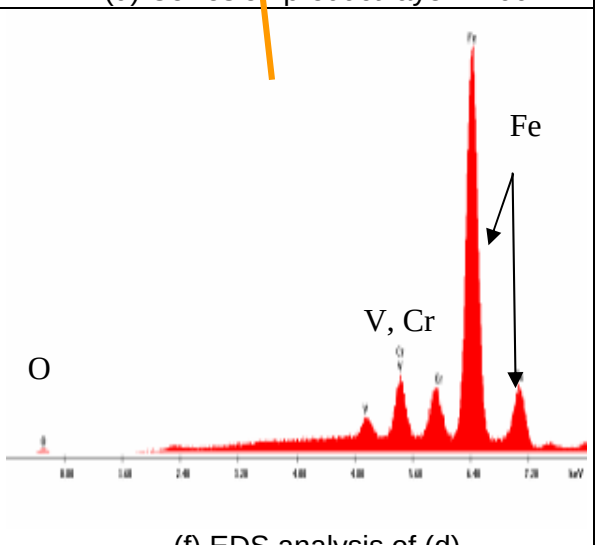

(f) EDS analysis of (d)

Figure 12 – Surface analysis with corrosion product / Free HAc= 1000 ppm (P_T: 3 bars, Vg= 5 m/s, pCO_2= 2 bars, T_g: 70°C, condensation rate= 0.25 mL/m^2/s)

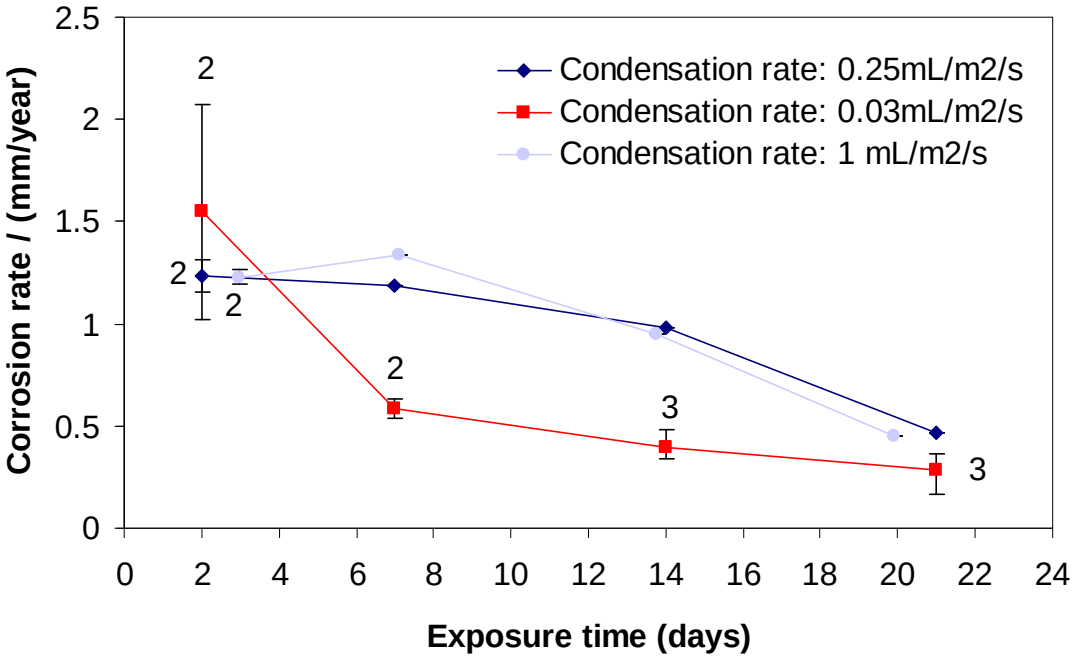

Figure 13: General corrosion – Effect of the condensation rate
pCO_2=3bars, T_g=70°C, $[HAc]_{free}$=0ppm, V_g=5m/s

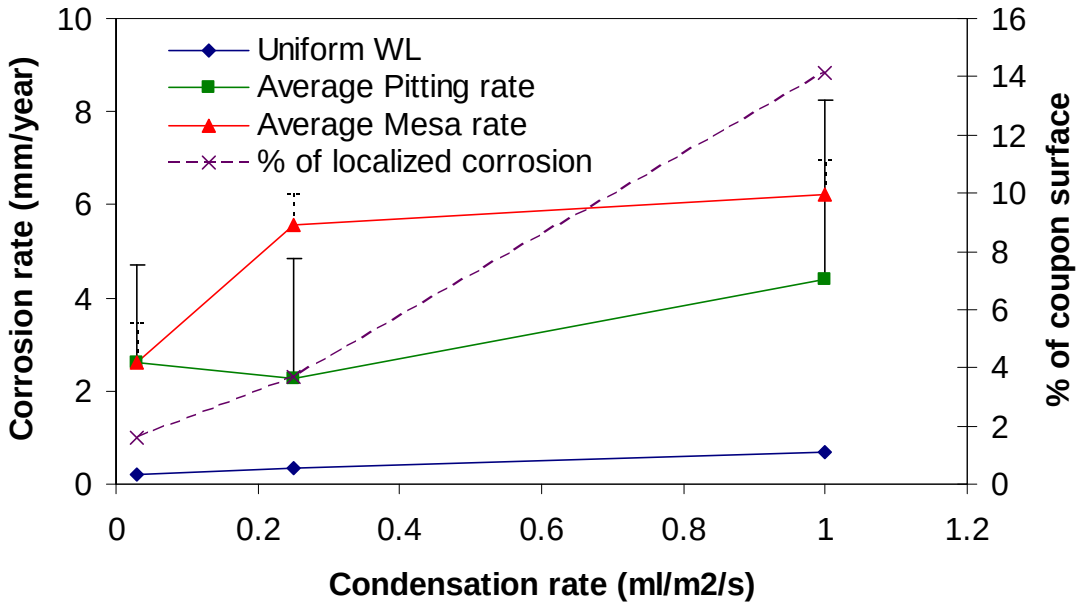

Figure 14: Localized corrosion - Effect of the condensation rate
pCO_2=3 bars, T_g=70°C, $[HAc]_{free}$=0 ppm, V_g=5 m/s

Surface profile Analysis

Top of the line - Exposure time: 21 days - After removal of the corrosion product layer

Scan of the coupon surface after removal of the corrosion product layer

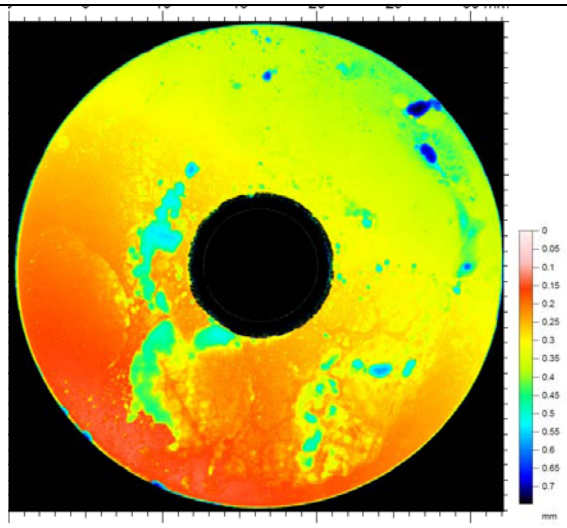

Mapping of the coupon surface showing localized corrosion

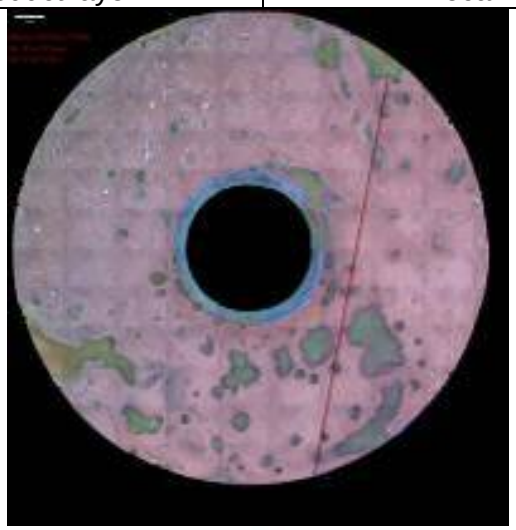

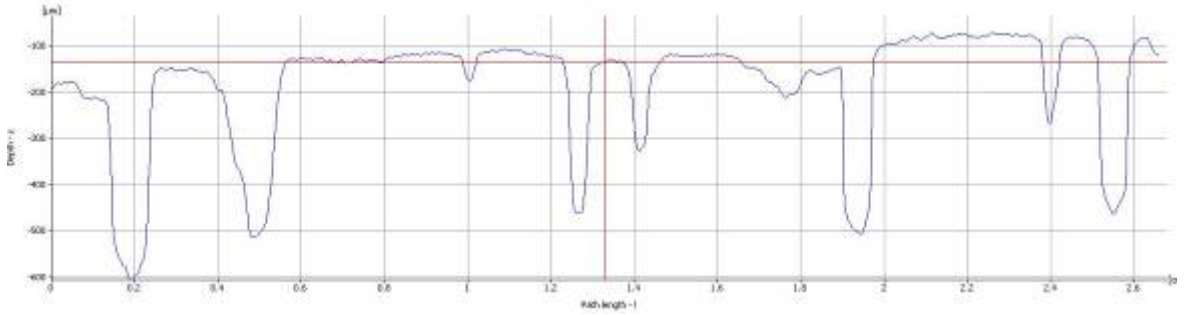

Surface profile along an arbitrary line (red line on the coupon picture)

Figure 15 – Surface analysis without corrosion product
Condensation rate= 1 mL/m^2/s
(P_T: 3 bars, Vg= 5 m/s , pCO_2= 2 bars, T_g: 70°C, Free HAc= 0 ppm)

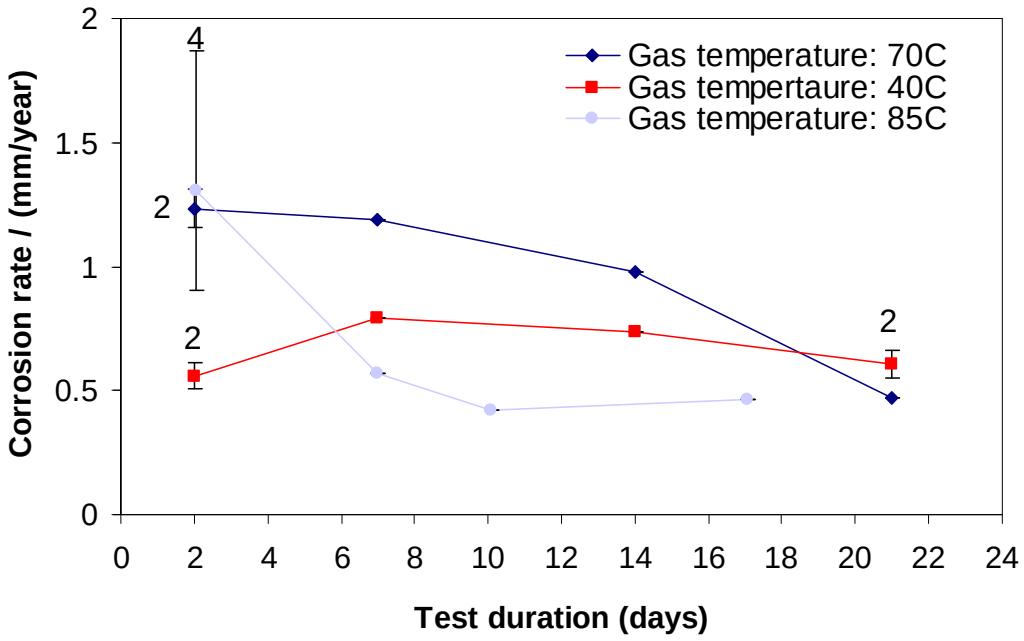

Figure 16: General corrosion – Effect of the gas temperature
pCO_2=3bars, $[HAc]_{free}$=0 ppm, V_g=5 m/s, Condensation rate=0.05 mL/m^2/s

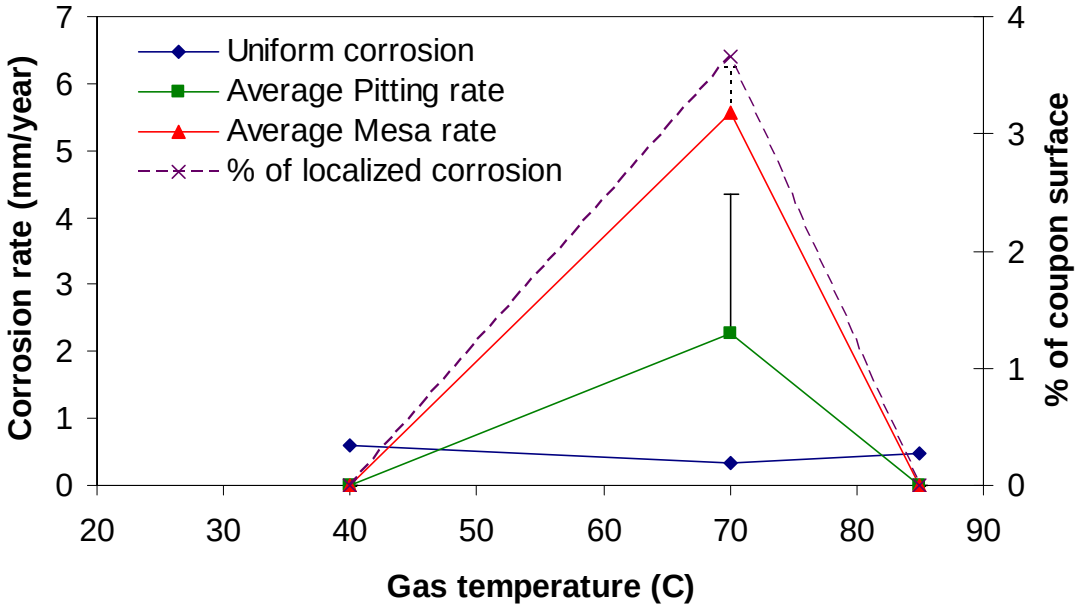

Figure 17: Localized corrosion - Effect of the gas temperature
pCO_2=3 bars, $[HAc]_{free}$=0 ppm, V_g= 5 m/s, Condensation rate=0.05 mL/m^2/s

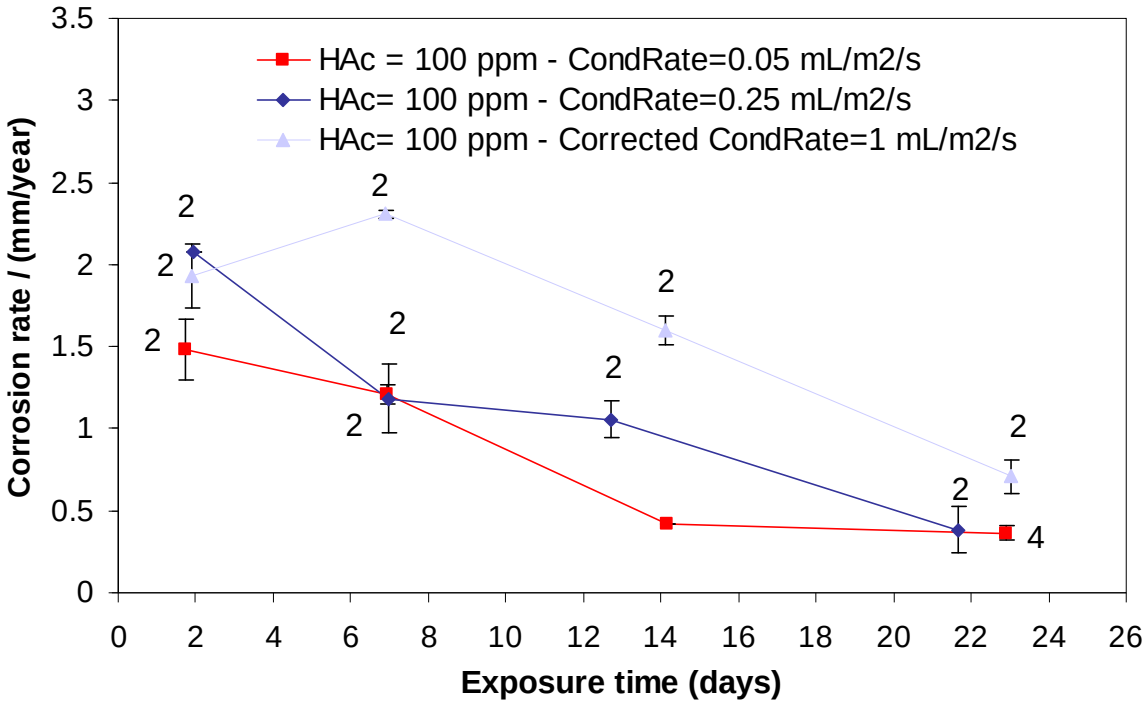

Figure 18: General Corrosion – Effect of HAc/Condensation rate
pCO_2=3bars, T_g=70ºC, V_g=5m/s
Set 1: Fixed $[HAc]_{free}$ = 100 ppm and
varying Condensation rate = 0.03, 0.25 and 1 mL/m^2/s

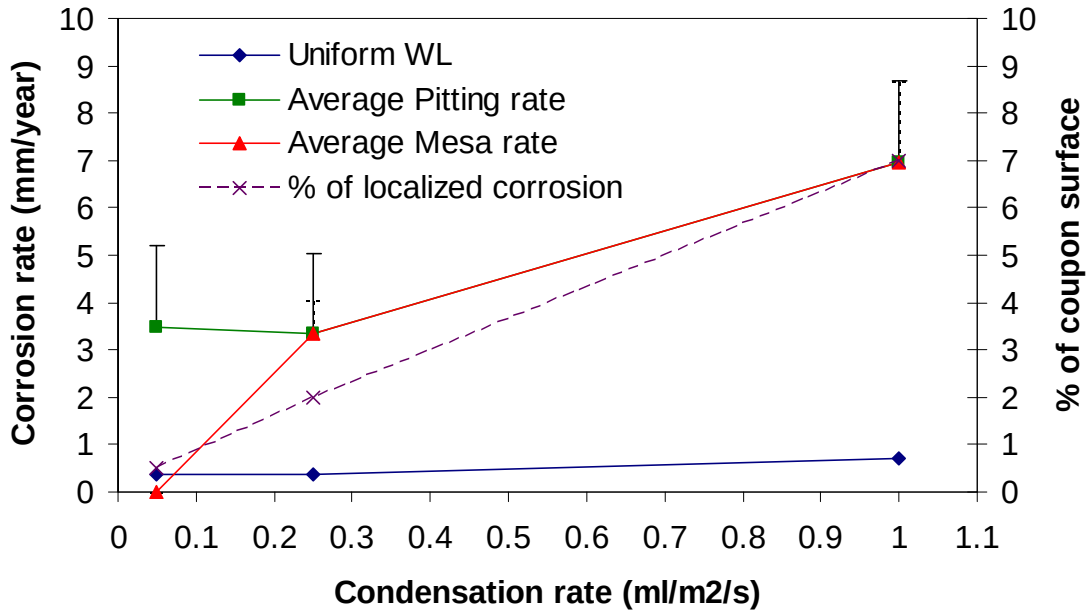

Figure 19: Localized corrosion - Effect of HAc/Condensation rate
pCO_2= 3b ars, T_g=70ºC, V_g=5m/s
Set 1: Fixed $[HAc]_{free}$ = 100 ppm and
varying Condensation rate = 0.03, 0.25 and 1 mL/m^2/s

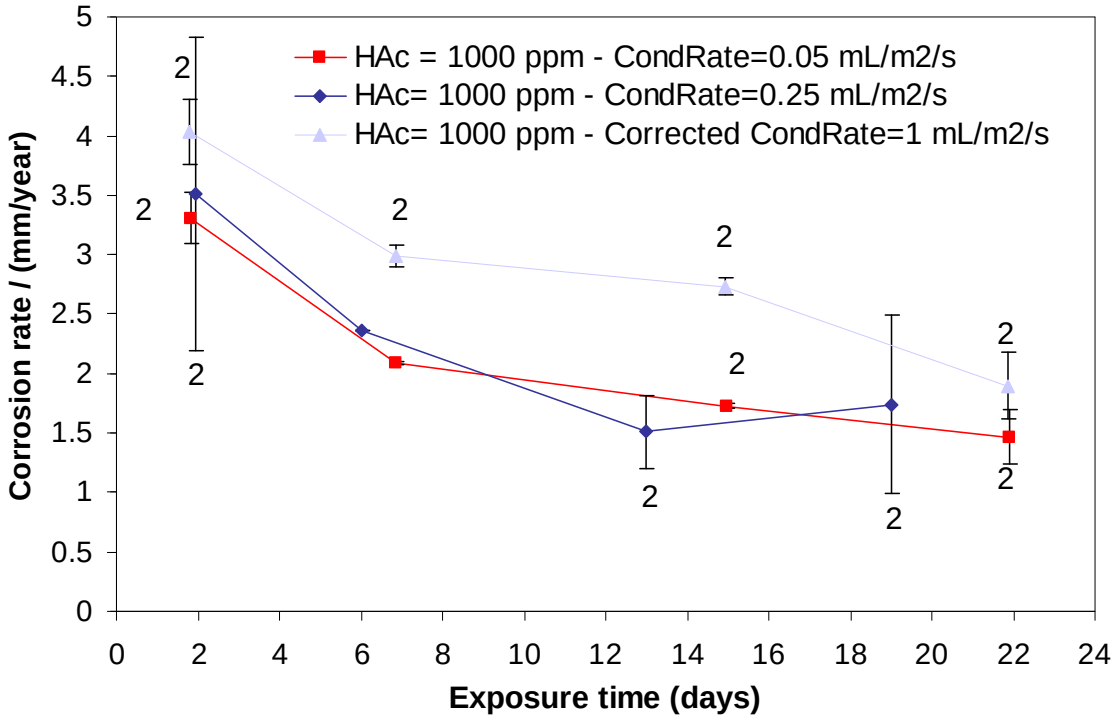

Figure 20: General corrosion - Effect of HAc/Condensation rate
pCO_2=3bars, T_g=70°C, V_g=5m/s
Set 2: Fixed $[HAc]_{free}$ = 1000 ppm and
varying Condensation rate = 0.03, 0.25 and 1 mL/m^2/s

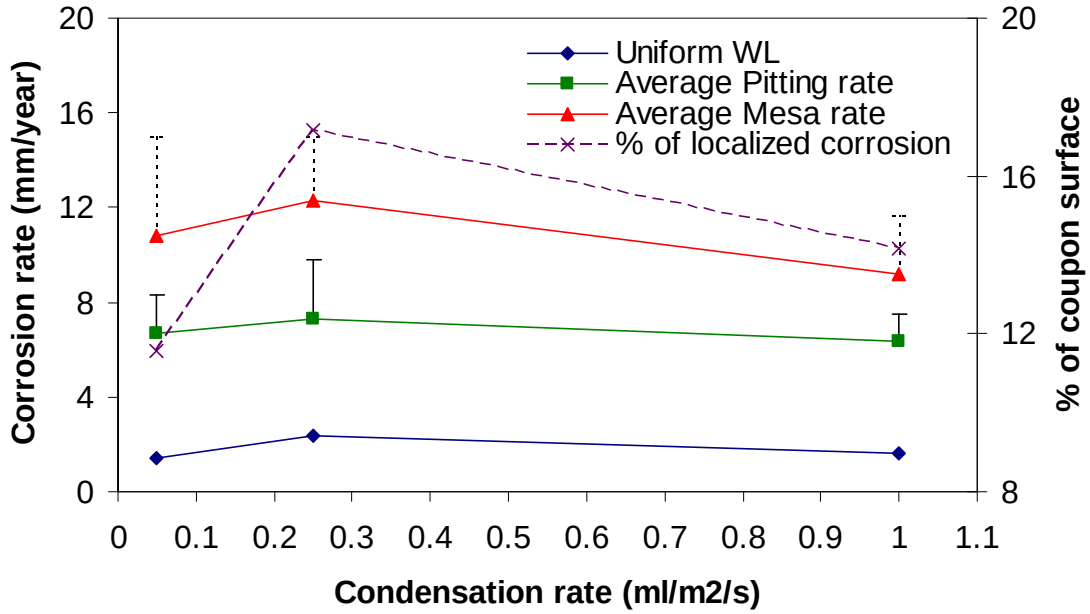

Figure 21: Localized corrosion - Effect of HAc/Condensation rate
pCO_2=3bars, T_g=70°C, V_g=5m/s
Set 2: Fixed $[HAc]_{free}$ = 1000 ppm and
varying Condensation rate = 0.03, 0.25 and 1 mL/m^2/s

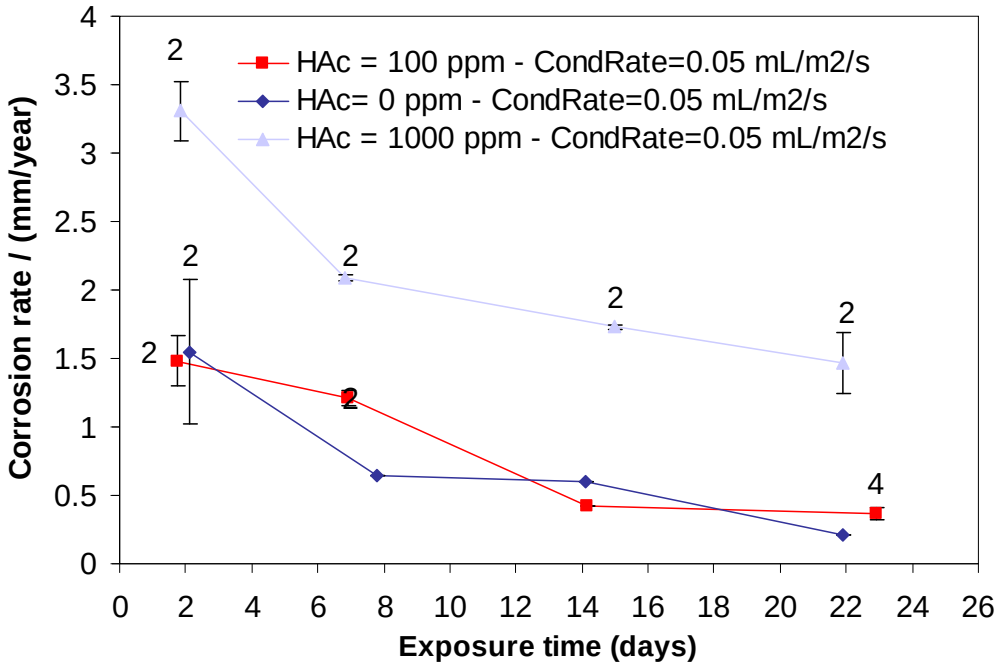

Figure 22: General corrosion – Effect of HAc/Condensation rate
pCO_2=3bars, T_g=70°C, V_g=5m/s
Set 3: Fixed Condensation rate = 0.05 mL/m²/s and varying $[HAc]_{free}$ = 0, 100, 1000 ppm

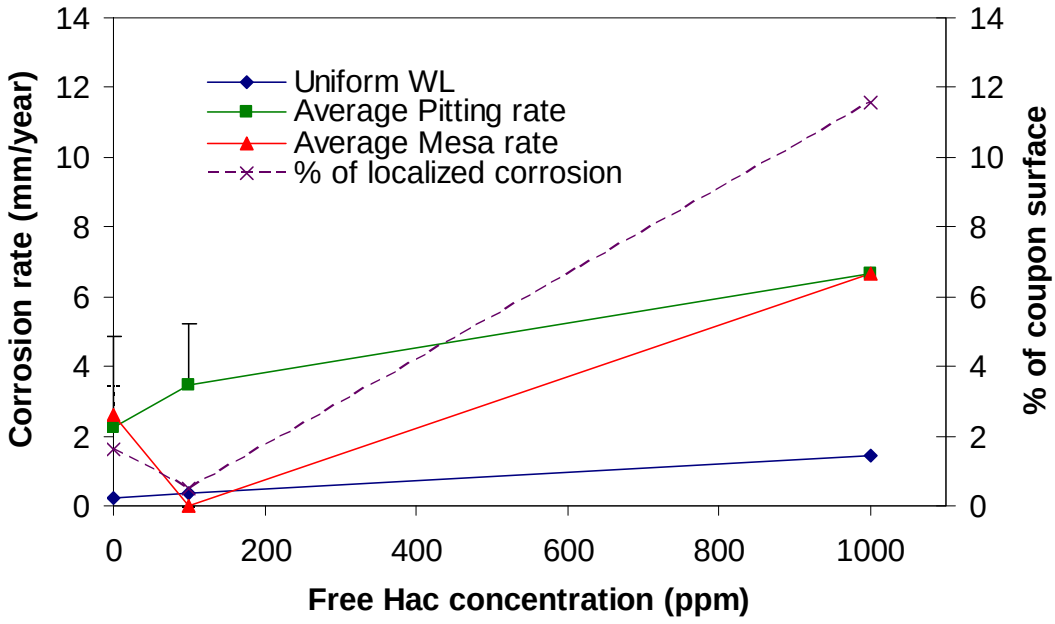

Figure 23: Localized corrosion - Effect of HAc/Condensation rate
pCO_2=3bars, T_g=70°C, V_g=5m/s
Set 3: Fixed Condensation rate = 0.05 mL/m²/s and varying $[HAc]_{free}$ = 0, 100, 1000 ppm

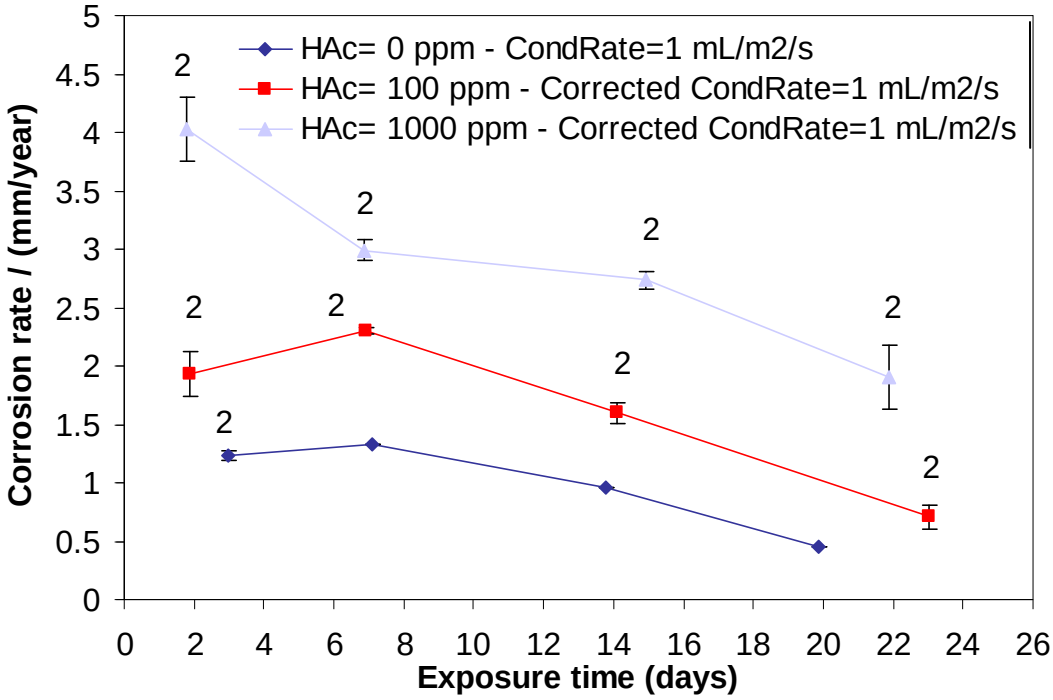

Figure 24: General corrosion – Effect of HAc/Condensation rate
pCO_2=3bars, T_g=70°C, V_g=5m/s
Set 4: Fixed Condensation rate = 1 mL/m^2/s and
varying $[HAc]_{free}$ = 0, 100, 1000 ppm

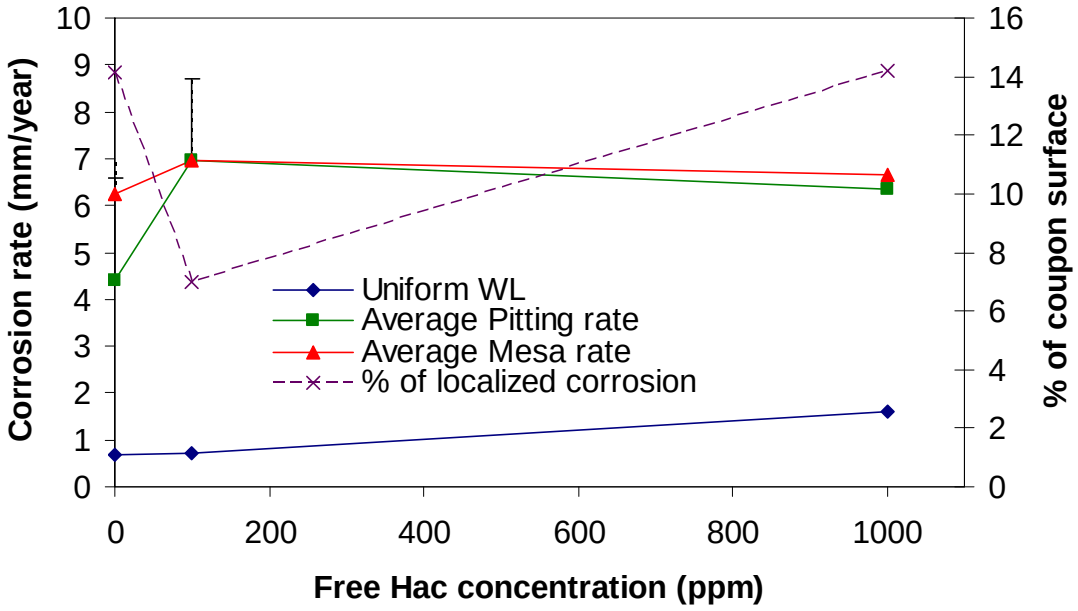

Figure 25: Localized corrosion - Effect of HAc/Condensation rate
pCO_2=3bars, T_g=70°C, V_g=5m/s
Set 4: Fixed Condensation rate = 1 mL/m^2/s and
varying $[HAc]_{free}$ = 0, 100, 1000 ppm

Surface profile Analysis

Top of the line - Exposure time: 21 days - After removal of the corrosion product layer

Scan of the coupon surface after removal of the corrosion product layer

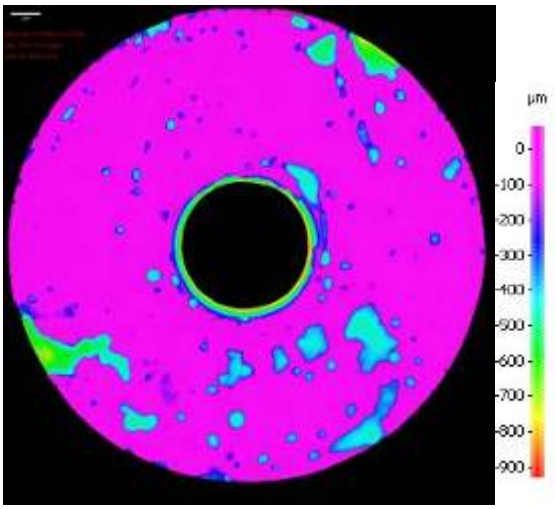

Mapping of the coupon surface showing localized corrosion

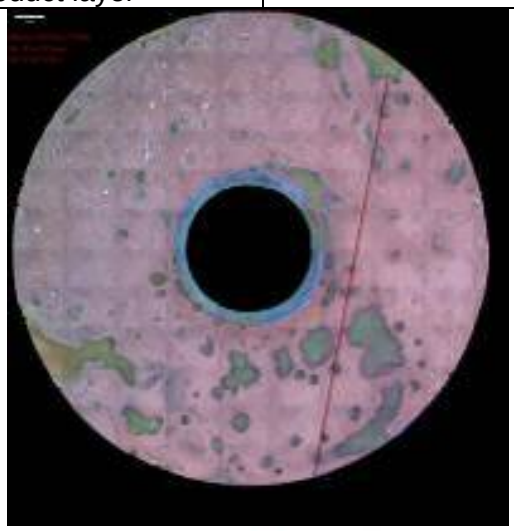

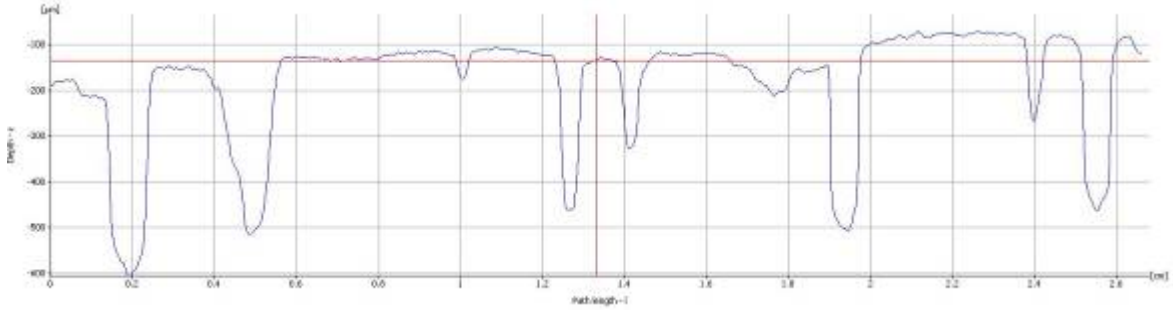

Surface profile along an arbitrary line (red line on the coupon picture)

Figure 26 – Surface analysis without corrosion product
Free HAc= 1000 ppm and condensation rate= 0.05 mL/m^2/s
(P_T: 3 bars, Vg= 5 m/s, pCO_2= 2 bars, T_g: 70°C)